Research Square

Preprints are preliminary reports that have not undergone peer review.
They should not be considered conclusive, used to inform clinical practice,
or referenced by the media as validated information.

Development, Hirshfeld surface analysis, DFT calculations and biological evaluation of Neratinib loaded Co-crystals for solubility enhancement

Rohit Sonawane
Indrayani Vidya Mandir's Krishnarao Bhegade Institute of Pharmaceutical Education and Research, Talegaon Dabhade, Tal- Maval,

Amol Rakte
amolsrakte@gmail.com

Indrayani Vidya Mandir's Krishnarao Bhegade Institute of Pharmaceutical Education and Research, Talegaon Dabhade, Tal- Maval,

Jyotiraditya Fiske
Indrayani Vidya Mandir's Krishnarao Bhegade Institute of Pharmaceutical Education and Research, Talegaon Dabhade, Tal- Maval,

Sanjay Arote
Indrayani Vidya Mandir's Krishnarao Bhegade Institute of Pharmaceutical Education and Research, Talegaon Dabhade, Tal- Maval,

Research Article

Keywords: Neratinib, Cocrystal, 3-Hydroxybenzoic acid, Solubility enhancement, HER2-positive breast cancer, Molecular docking, DFT, Factorial design

Posted Date: July 7th, 2026

DOI: https://doi.org/10.21203/rs.3.rs-9392522/v1

License: This work is licensed under a Creative Commons Attribution 4.0 International License.
Read Full License

Additional Declarations: No competing interests reported.

Development, Hirshfeld surface analysis, DFT calculations and biological evaluation of Neratinib loaded Co-crystals for solubility enhancement.

Rohit Sonawane[a], Amol S.Rakte[*a,1], Jyotiraditya Fiske[b], Sanjay R.Arote[c]

[a,b] Department Of Pharmaceutics, Indryani Vidya Mandirs Krishnarao Bhegade Institute of Pharmceutical Education and Research, Talegaon Dabhade, Tal-Maval, Pune-410507, Maharashtra, India

[c] Department Of Pharmacology, Indryani Vidya Mandirs Krishnarao Bhegade Institute of Pharmceutical Education and Research, Talegaon Dabhade, Tal-Maval, Pune-410507, Maharashtra, India

***Corresponding Author:**

[a,1]Amol S. Rakte [*]

Department Of Pharmaceutics, Indryani Vidya Mandirs Krishnarao Bhegade Institute of Pharmceutical Education and Research, Talegaon Dabhade, Tal-Maval, Pune-410507, Maharashtra, India

Email: amolsrakte@gmail.com

Orcid ID – 0009-0000-2359-1438

ABSTRACT

Objectives: Neratinib, a pan-HER tyrosine kinase inhibitor for HER2-positive breast cancer, suffers from extremely poor aqueous solubility (<0.002 mg/mL), severely limiting oral bioavailability and therapeutic efficacy. This study aimed to develop and optimize neratinib cocrystals using rational co-former selection and factorial design to enhance solubility, dissolution, and anticancer activity.**Methods:** Five potential co-formers were screened at 3 molar ratios (1:1, 1:2, 1:3) using SynthonDock software. Electronic properties and interaction energetics were characterized using density functional theory (DFT) calculations at B3LYP/6-31G(d,p) level. Neratinib–3-hydroxybenzoic acid cocrystals were prepared by solvent evaporation and optimized in 3^2 factorial design using the concentration of co-former (24.8–74.4 mg) and stirring time (30–90 min) as independent variables. The PXRD, FTIR, DSC, SEM and Hirshfeld surface studies were carried out to characterize the compounds. MTT assay was used to evaluate in vitro cytotoxicity against SK-BR-3 cells. **Results**: 3-Hydroxybenzoic acid showed the best binding energy (−10.05 kcal/mol with a ratio of 1:3) and highest co-crystal score (90.5). Increased reactivity was established using density functional theory (DFT) with the calculation showing diminished HOMO–LUMO gap (0.4324 eV vs 3.3072 eV for pure drug). The 12.4-fold solubility enhancement (0.112 mg/mL vs 0.009 mg/mL) and 4.6 times better dissolution (84.6% vs 18.4% at 60 min) was reached using the third batch PF9 (74.4 mg of 3-hydroxybenzoic acid, 90 minutes.) Cytotoxicity studies showed enhanced anticancer activity (IC_{50} = 18.46 µg/mL vs 24.18 µg/mL for pure neratinib) toward HER2-positive breast cancer cells. **Conclusion:** The optimized neratinib–3-hydroxybenzoic acid cocrystal is a clinically relevant pharmaceutical approach to enhance oral bioavailability and therapeutic efficacy in HER2-positive breast cancer for subsequent biological exploration in vivo.

Keywords: Neratinib; Cocrystal; 3-Hydroxybenzoic acid; Solubility enhancement; HER2-positive breast cancer; Molecular docking; DFT; Factorial design.

INRODUCTION

Breast cancer is one of the most common and lethal cancers globally, with around 2.3 million new cases and more than 685,000 deaths diagnosed annually, making it the leading cause of cancer death among women worldwide[1]. A key sub-type, HER2-positive breast cancer accounts for almost 15–20% of all subtypes (of breast cancer) that are characterized by aggressive tumor progression, rapid metastasis and significantly inferior survival outcomes when compared to HER2-negative disease[2]. Despite significant progress in targeted oncology therapeutics, HER2-positive and hormone receptor-positive breast cancers remain clinically challenging and similarly resistant to therapy[3]. HER2-targeted therapies, such as trastuzumab and lapatinib have prompted the emergence of acquired resistance, dose-limiting toxicities, and poor central nervous system penetration. Indirect costs are incurred through lost productivity and long-term supportive care, resulting in a total cost burden of over USD 200 billion per year worldwide for the management of breast cancer[4]. The need to develop better, cost-effective and orally bioavailable treatment approaches for HER2-positive malignancies is further emphasized by the escalating incidence rates particularly in low- and middle-income countries along with restricted access to high-cost therapies[5].

Neratinib is a small molecular inhibitor of human epidermal growth factor receptor (HER) family tyrosine kinase, which acts on HER1, HER2, and HER4 receptors by covalent binding to the ATP-binding site of these receptors and blocking downstream oncogenic signaling cascades (RAS/MAPK and PI3K/AKT pathways) involved in driving tumor cell growth, survival, and metastasis[6]. Neratinib, chemically known as (E)-N-[4-[[3-chloro-4-[(pyridin-2-yl)methoxy]phenyl]amino]-3-cyano-7-ethoxyquinolin-6 -yl]-4-(dimethylamino)but -2-enamide, has a molecular formula of $C_{30}H_{29}ClN_6O_3$ and a weight of 557.04 g/mol. Its irreversible action mechanism offers a unique therapeutic benefit compared to reversible inhibitors by inducing persistent HER pathway inhibition and overcoming resistance mutations[7]. Clinical benefit of neratinib in extended adjuvant treatment of HER2-positive early breast cancer has been demonstrated in the ExteNET phase III clinical study[8]. On the other hand, neratinib is classified as a BCS Class II drug and suffers from extremely low aqueous solubility (< 0.002 mg/mL at physiological pH) leading to limited oral bioavailability, heterogeneous biological response and poor patient adherence, calling for an immediate pharmaceutical intervention to enhance its biopharmaceutical performance[9].

Cocrystal engineering presents both sound science and pharmaceutical viability as a solid state modification approach to reduce the solubility limitations of Biopharmaceutics Classification System (BCS) Class II drugs without chemical alteration of the covalent molecular structure or pharmacological activity[10]. Pharmaceutical cocrystals, also known as hydrogen bonded cocrystals or simply pharmaceutical co-crystals, are crystalline (a single-phase) materials composed of an active pharmaceutical ingredient and a pharmaceutically acceptable co-former that is held together by non-covalent intermolecular interactions at ambient conditions, such as hydrogen bonding, π–π stacking interactions and van der Waals forces[11]. Different from salt formation, cocrystallization does not require ionizable functional groups and is therefore applicable to a much larger variety of drug molecules. Specifically, cocrystal formation with judiciously selected Generally Recognized as Safe

(GRAS) co-former molecules of nicotinamide, succinic acid, maleic acid and fumaric acid has been shown to dramatically increase drug solubility/dissolution rate/stability/oral bioavailability[12]. Recent developments in cocrystal screening protocols such as solvent evaporation, liquid-assisted grinding and slurry techniques have continued to speed the process of rational cocrystal design. The full characterization through DSC, FTIR, PXRD and SEM provides mechanistic understanding of the nature of drug–co-former interactions as well as solid-state properties of the respective cocrystal systems[13].

The goal of the current study is to design and characterize pharmaceutical cocrystals of neratinib with various co-formers that can improve solubility and dissolution by a considerable extent. Goals are focused on co-former screening, cocrystal preparation via solvent evaporation and structured physicochemical characterization. In vitro drug release profiles and a rational foundation for neratinib enhanced oral bioavailability in therapy of HER2(+) breast cancer are also evaluated.

MATERIALS AND METHODS

MATERIALS

Neratinib (purity ≥98%, molecular weight 557.04 g/mol) was gifted as samples from Sciquaint Innovations Pvt. Ltd., Pune, India. 3-Hydroxybenzoic acid (analytical grade, ≥99% purity, M.W.138.12 g/mol) was purchased from Sciquaint Chemicals, Pune, India. Nicotinamide (analytical grade, purity ≥98%), succinic acid (analytical grade, purity ≥99%), maleic acid (analytical grade, purity ≥99%), fumaric acid (analytical grade, purity≥99%), potassium dihydrogen phosphate (analytical grade), disodium hydrogen phosphate (analytical grade) and sodium lauryl sulfate(analytical grade). Methanol (HPLC grade), acetone (analytical grade) and hydrochloric acid (analytical grade, 37%) were obtained from Neeta Chemicals, Pune, India. Throughout the study, double distilled water was employed. All other chemicals and reagents were of analytical grade and used as received.

METHODS

Calibration Curve Determination of Neratinib

Calibration curve to establish the linear relationship between concentration and absorbance of neratinib at λmax 264 nm in methanol. Stock primary solution (1000 µg/mL) was prepared by dissolving 10 mg of neratinib in methanol with sonication (Oscar Ultrasonics, Mumbai, India), and working standard solutions were prepared as follows: 2, 4, 6, 8, 10 and 12 µg/mL by suitable dilution with phosphate buffer pH 6.8. The absorbance of each solution was recorded in triplicate (n = 3) at 264 nm against blank using a UV–visible spectrophotometer (UV-1800, Shimadzu, Japan) with quartz cuvettes of path length 1 cm. A calibration graph was constructed by plotting absorbance against concentration and data were analyzed through linear regression ($y = mx + c$) to ascertain the slope, intercept, and correlation coefficient (r^2). Linearity was assessed according to the ICH Q2(R1) guidelines and $r^2 \geq 0.999$ was taken as acceptable[14].

Solubility Study of Pure Neratinib

To characterize the dissolution behavior of neratinib and inform selection of co-former for cocrystal development, the equilibrium solubility of neratinib was measured in physiologically relevant media and organic solvents. An excess amount of neratinib (50 mg) was suspended in 10 mL of each solvent distilled water, phosphate buffer pH 6.8, phosphate buffer pH 7.4, 0.1 N HCl, methanol, ethanol, acetone and acetonitrile in different 25 mL stoppered conical flasks. The flasks were agitated to saturation equilibrium at 25 ± 2°C and 100 g in a thermostatic orbital shaker (Labline, Mumbai, India) for 24 h before settling for 30 min. The supernatant was filtered using a Whatman filter paper No. 41, appropriately diluted and the absorbance of the solution measured at λ_{max} 264 nm with UV-Visible spectrophotometer (UV-1800 Shimadzu, Kyoto Japan)[15].

Molecular Docking of Neratinib with Co-formers

Molecular docking was performed to predict intermolecular interaction feasibility between neratinib and five candidate co-formers nicotinamide, succinic acid, maleic acid, fumaric acid, and 3-hydroxybenzoic acid at three molar ratios (1:1, 1:2, and 1:3) using SynthonDock v1.0 (Geinforce Technology, Pune, India) employing AutoDock Vina scoring function. The three-dimensional structure of neratinib (PubChem CID: 9915743) was retrieved in SDF format and converted to PDB format using Avogadro v1.2.0. Co-former structures were similarly retrieved and prepared with hydrogen atoms added and energy-minimized using the MMFF94 force field. Docking parameters were set with Exhaustiveness = 16, Number of Modes = 9, and Energy Range = 5.0 kcal/mol. Grid box dimensions and center coordinates were set independently for each molar ratio run: 1:1 ratio (45.2 × 42.3 × 36.8 Å; center: 7.27, −3.94, 3.98 Å), 1:2 ratio (42.7 × 41.5 × 41.0 Å; center: 7.13, 5.23, −1.34 Å), and 1:3 ratio (42.4 × 40.6 × 41.2 Å; center: 4.24, −3.47, −0.68 Å). The best-pose binding affinity (kcal/mol), co-crystal score, number of hydrogen bonds, H-bond distances (Å), and bond types were extracted from the top-ranked docking pose (Pose 0) for each co-former at each ratio. Co-formers with the most negative binding affinity, highest co-crystal score, and greatest number of H-bonds were shortlisted for experimental preliminary trial batches[16].

Preliminary Trial Batches for Co-former Selection

Three computationally shortlisted co-formers (3-hydroxybenzoic acid, nicotinamide and succinic acid) were experimentally validated in preliminary trial batches of neratinib cocrystals prepared by solvent evaporation at molar ratios of 1:1, 1:2, and 1:3. Neratinib (100 mg per batch) and the respective co-former were accurately weighed at the specified molar ratio, followed by dissolution in acetone (analytical grade from SD Fine-Chem, Mumbai, India) in a 25 mL glass beaker and magnetic stirring (Remi Instruments, Mumbai, India) at 500 rpm and 25 ± 2°C until a clear solution formed (~30 min), then left for slow evaporation at room temperature (25 ± 2°C) under laminar air-flow. The dried residue (40°C, 12 h) was sieved through BSS mesh 60 (250 μm) and characterized for: (a) solubility in phosphate buffer pH 6.8 at λmax (mg/mL (n = 3) using a UV-Visible spectrophotometer (UV-1800, Shimadzu, Kyoto)) at 264 nm and (b) melting point using the open capillary method with a Sunbim Instruments apparatus (Ambala)). The co-formers and molar ratios showing the

greatest solubility enhancement with a detected melting point shift were selected for DFT analysis and further optimization using a 32 factorial design[17].

Table 1: Preliminary Trial Batches Co-former Screening and Molar Ratio Optimization

Batch Code	Co-former	Molar Ratio (Neratinib:Co-former)	Solubility in PBS pH 6.8 (mg/mL, mean ± SD)	Melting Point (°C)	Cocrystal Formation Inference
T1	Nicotinamide	1:1	0.031 ± 0.002	169–171	Partial
T2	Nicotinamide	1:2	0.074 ± 0.003	161–163	Confirmed
T3	Nicotinamide	1:3	0.069 ± 0.003	162–164	Confirmed
T4	Succinic Acid	1:1	0.028 ± 0.002	173–175	Partial
T5	Succinic Acid	1:2	0.051 ± 0.002	164–166	Confirmed
T6	Succinic Acid	1:3	0.048 ± 0.003	166–168	Confirmed
T7	3-Hydroxybenzoic Acid	1:1	0.041 ± 0.003	168–170	Partial
T8	3-Hydroxybenzoic Acid	1:2	0.112 ± 0.005	152–154	Confirmed
T9	3-Hydroxybenzoic Acid	1:3	0.096 ± 0.004	154–156	Confirmed
T10	3-Hydroxybenzoic Acid	1:4	0.088 ± 0.004	156–158	Confirmed

All values are presented as mean ± SD (n=3). Of the three shortlisted co-formers, 3-hydroxybenzoic acid at a molar ratio of 1:2 (T8) showed the highest solubility (0.112 ± 0.005 mg/mL) which correlated with strongest binding energy from docking studies −6.16 kcal/mol at a 1:2 conformer with four H-bonds and highest score of co-crystal complex, i.e., 58.5, for molecular docking studies. The molar ratio of 1:1 to 1:3 was used as the factor levels for independent variable X1, while 3-hydroxybenzoic acid was thereby chosen as the single co-former for applied DFT study and also the experimental studies based on combined response with a 3^2 factorial design.

Density Functional Theory (DFT) Analysis of Neratinib–3-Hydroxybenzoic Acid Complex

To investigate the electronic properties, molecular reactivity, and interaction energetics of the optimized neratinib–3-hydroxybenzoic acid binary system at the desired molar ratio (1:2), theoretical calculations were only carried out using DFT on this adduct using ORCA v5.0.3 (Frank Neese, MPI für Kohlenforschung, Germany), molecular structure preparations and visualisations were carried out in Avogadro v1.2.0. Full geometry optimization of neratinib, 3-hydroxybenzoic acid, and the neratinib–3-hydroxybenzoic acid 1:2 complex was carried out in the gas phase at the level of theory using B3LYP/6-31G(d,p). Global reactivity descriptors obtained from frontier molecular orbital energies were as follows: HOMO energy (E_HOMO), LUMO energy (E_LUMO), HOMO–LUMO energy gap (ΔE = E_LUMO −

E_HOMO), chemical hardness ($\eta = \Delta E/2$), chemical softness ($S = 1/2\eta$), electronegativity ($\chi = -(E_HOMO + E_LUMO)/2$), chemical potential ($\mu = (E_HOMO + E_LUMO)/2$) and electrophilicity index $\omega=(\mu^2/2\eta)$. In order to identify complementary electropositive and electronegative regions that dictate drug–co-former H-bond formation, molecular electrostatic potential (MEP) maps were calculated at the same level of theory. The interaction energy (ΔE_int) of the binary complex was calculated as:

$$\Delta E_int = E_complex - (E_neratinib + 2 \times E_3\text{-}HBA)$$

where basis set superposition error (BSSE) correction was applied using the counterpoise method. Vibrational frequency analysis confirmed absence of imaginary frequencies, validating all optimized structures as true energy minima[18,19].

Experimental Design for Optimization of Neratinib-3-Hydroxybenzoic Acid Cocrystals

So, to optimize the preparation of neratinib–3-hydroxybenzoic acid cocrystals, a full factorial design 3^2 was employed to study the influence of two independent variables drug:co-former molar ratio (X1) and agitation time during cocrystallization (X2) on cocrystal yield while employing Design-Expert® software v13.0 (Stat-Ease Inc., Minneapolis, USA). Each variable was investigated at three levels namely low (−1), medium (0) and high (+1), resulting in nine experimental batches (PF1–PF9). Selected dependent responses were equilibrium solubility in phosphate buffer (pH 6.8) (Y1, mg/mL; target: maximize), and cumulative % drug release at 60 min (Y2, %; target: maximize) as given in table 2. A fitted second-order polynomial equation was used:

$$Y = b_0 + b_1X1 + b_2X2 + b_{12}X1X2 + b_{11}X1^2 + b_{22}X2^2$$

where Y is the response measured; b_0 is intercept; b_1, b_2 are linear coefficients; and b12 is the interaction coefficient and b_{11}, b_{22} quadratic coefficients. Statistical significance ($p < 0.05$) was assessed using ANOVA. R^2, adjusted R^2 and predicted R^2 were used to evaluate model fit. Contour plots and 3D response surface plots were further constructed based on the analysis of variance to identify the effects of each variable on responses[20].

Table 2: Independent Variables and Levels for 3^2 Factorial Design

Independent Variable	**Symbol**	**Low (−1)**	**Medium (0)**	**High (+1)**
Concentration of 3-hydroxybenzoic acid (mg/100 mg neratinib)	X1	24.8	49.6	74.4
Stirring time during cocrystallization (min)	X2	30	60	90
Dependent Variable		**Goal**		
Equilibrium solubility in PBS pH 6.8 (mg/mL)	Y1	Maximize		
Cumulative % drug release at 60 min	Y2	Maximize		

Table 3: Formulation Table actual composition of all experimental co-crystal batches

Batch	**Neratinib (mg)**	**3-Hydroxybenzoic Acid (mg) (X1)**	**Stirring Time (min) (X2)**	**Acetone (mL)**

PF1	100	24.8	30	q.s. 10
PF2	100	24.8	60	q.s. 10
PF3	100	24.8	90	q.s. 10
PF4	100	49.6	30	q.s. 10
PF5	100	49.6	60	q.s. 10
PF6	100	49.6	90	q.s. 10
PF7	100	74.4	30	q.s. 10
PF8	100	74.4	60	q.s. 10
PF9	100	74.4	90	q.s. 10

3-Hydroxybenzoic acid MW = 138.12 g/mol; Neratinib MW = 557.04 g/mol. Quantities calculated based on stoichiometric molar ratios. Acetone (analytical grade, SD Fine-Chem, Mumbai, India) used as cocrystallization solvent; q.s. = quantity sufficient.

Preparation of Neratinib–3-Hydroxybenzoic Acid Co-crystals

Cocrystals of neratinib–3-hydroxybenzoic acid (PF1–PF9) were formed using the solvent evaporation method according to 3^2 factorial design as per table 3. Neratinib (100 mg) and 3-hydroxybenzoic acid were co-dissolved in acetone (analytical grade, SD Fine-Chem, Mumbai, India) in a 25 mL glass beaker at the molar ratio described in Table 1 with continuous magnetic stirring at 500 rpm (Remi Instruments, Mumbai, India) at a temperature of 233 ± 2 °C for the time period specified for each batch (30, 60, or 90 min). The solution was transferred to a petri dish and left for slow evaporation at room temperature (25 ± 2 °C) in a laminar airflow cabinet to yield the crystalline solid. The crystalline mass was dried at 40°C for 12 h in a hot air oven (Narang Scientific, New Delhi, India), triturated and passed through BSS mesh 60 (250 μm), and stored in airtight amber glass vials at 25 ± 2°C/60% RH until characterization[21].

Characterization of Neratinib-3-Hydroxybenzoic Acid Cocrystals

Melting Point Determination

Melting points of pure neratinib, 3-hydroxybenzoic acid, physical mixture and cocrystal batches PF1–PF9 were determined using open capillary method in digital melting point apparatus (Sunbim Instruments, Ambala, India) at a heating rate of 2°C/min. Results are shown as mean ± SD (n = 3)[22].

Fourier Transform Infrared Spectroscopy (FTIR)

FTIR spectra of neratinib, 3-hydroxybenzoic acid, physical mixture and optimized cocrystal were analyzed using an IR Affinity-1S spectrophotometer (Shimadzu, Kyoto, Japan). KBr pellets were formed by mixing 2 mg of sample with 200 mg spectroscopic grade KBr, and compressed at 10 tonnes (Techno Search Instruments, Mumbai, India). Spectra were collected between 400–4000 cm^{-1} at 4 cm^{-1} resolution using 32 scans. Characteristic peak shifts or disappearances indicative of drug–co-former hydrogen-bond interactions were detected through overlay comparison[23].

Powder X-ray Diffractometry (PXRD)

The PXRD patterns of pure neratinib, 3-hydroxybenzoic acid, physical mixture and cocrystal batches were obtained using a Miniflex 600 diffractometer (Rigaku Corporation, Tokyo, Japan) with Cu-Kα radiation (λ = 1.5406 Å), operating at 40 kV and 15 mA. Data were collected over the 2θ range of 5°–50° at a scan speed of 2°/min with step size 0.02°. Changes such as the emergence of new diffraction peaks or dislocation of a characteristic peak corresponding to an active pharmaceutical ingredient (API) were observed, which are indicative of formation of the new solid-state phase[24].

Differential Scanning Calorimetry (DSC)

The thermal behavior of pure neratinib, 3-hydroxybenzoic acid, physical mixture and cocrystals was studied on a DSC-60 Plus (Shimadzu, Kyoto, Japan). Samples (3–5 mg) were crimped in perforated aluminum pans and subjected to a ramp from 30°C to 300°C at 10°C/min under nitrogen purge at 50 mL/min, using an empty aluminum pan as reference. Cocrystal formation was confirmed by a single endotherm distinct from individual components[25].

Scanning Electron Microscopy (SEM)

The surface morphology of pure neratinib and optimized cocrystals was examined by using EVO 18 scanning electron microscope (SEM) (Zeiss, Germany) at an accelerating voltage ranging between 10–15 kV. Liquid samples were fixed onto metallic stubs with a double-sided carbon tape and coated with Au–Pd (60:40) for 90 s in argon atmosphere (Quorum Q150T, UK). Photomicrographs were taken at ×500, ×1000 and ×5000[26].

Hirshfeld Surface Analysis

The Hirshfeld surface analysis of the optimized neratinib–3-hydroxybenzoic acid cocrystal was carried out by using CrystalExplorer v21. 5 to map intermolecular interactions. The d_norm surface was calculated using a color scale ranging from −0.5 to +1.5 a.u, atom types for donors and acceptor set to "Any" with a Van der Waals radii tolerance of 0.00 Å respectively, two-dimensional fingerprint plots were obtained, allowing us to quantify the proportion of H···O, H···H and C···H intermolecular contacts relative to the total surface area of the Hirshfeld surface.

Equilibrium Solubility Study

Equilibrium solubility of neat neratinib and cocrystal PF1–PF9 batches was assessed in phosphate buffer (pH 6.8) at 25 ± 2°C; the excess sample (~50 mg equivalent drug) was added to 10 mL buffer in stoppered conical flasks and agitated for 24 h at a rate of 100 rpm on a thermostatic orbital shaker (Remi Instruments, Mumbai, India), followed by a settling period of 30 min. Supernatant was filtered using Whatman No. 41 filter paper, and the absorbance recorded at λmax 264 nm (UV-1800 Shimadzu; Kyoto, Japan). Solubility was determined from a calibration curve (n = 3, mean ± SD, mg/mL)[27].

In Vitro Drug Release Study

Release of drug from the cocrystal batches PF1–PF9 and pure neratinib was performed using USP Type II Dissolution Apparatus, paddle method (Electrolab TDT-08L, Mumbai, India) at 37 ± 0.5 °C; 75 rpm in phosphate buffer pH 6.8 solution with sodium lauryl sulfate 0.5% w/v in a total volume of 900 mL. Samples for each of the three experiments were equivalent to 240 mg neratinib/vessel. Aliquots of 5 mL were removed at time points 5, 10, 15, 20, 30, 45 and 60 min and replaced with an equal volume of fresh pre-warmed medium. Samples were filtered and diluted, and absorbance was determined with λmax 264 nm. From the calibration curve, cumulative percentage drug release was computed (n=3 mean ± SD)[28].

Drug Content Determination

A quantity equivalent to 10 mg of neratinib was suspended in 100 mL methanol and sonicated for 30 min (Oscar Ultrasonics, Mumbai, India), filtered through Whatman No. 41, diluted with phosphate buffer pH 6.8 and absorbance was measured at λmax [264 nm] (UV-1800, Shimadzu, Kyoto, Japan). The level of the drug was calculated from the calibration curve and expressed as % label claim (n = 3). Acceptance criterion: 98–102%[29].

Stability Studies

Stability studies for optimized cocrystal batch were performed under accelerated conditions according to ICH Q1A(R2) guidelines at 40°C/75% RH for 3 months using stability chamber (Thermolab, Mumbai, India). At 0, 1, 2, and 3 months, samples were withdrawn and assessed for visual aspect, drug content, equilibrium solubility and PXRD pattern. Statistical significance of changes was evaluated by one-way ANOVA ($p < 0.05$) with the use of GraphPad Prism v9.0[30].

In Vitro Cytotoxicity Study (MTT Assay)

MTT [3-(4,5-dimethylthiazol-2-yl)-2,5-diphenyltetrazolium bromide] assay was used to measure the dose dependent cytotoxic activity of pure neratinib, 3-hydroxybenzoic acid and optimized cocrystal batch PF9 against SK-BR-3 (HER2-positive human breast cancer) cell line. Then, SK-BR-3 cells were cultured in McCoy's 5A medium with 10% fetal bovine serum (FBS) and 1% penicillin-streptomycin at 37°C with 5% CO_2. Cells were plated in a 96-well plate at the density of 1×10^4 cell/well and incubated for 24 h to allow adherence. Test samples were prepared in DMSO and serially diluted to six concentrations (1, 5, 10, 25, 50 and 100 µg/mL) in culture medium (final DMSO ≤ 0.1% v/v). Treatment medium was aspirated 48 h after and MTT solution (5 mg/mL in PBS, 20 µL/well) was added then incubated for 4 h at 37 °C. Formazan crystals were dissolved in DMSO (150 µL/well), the absorbance was read using a microplate reader (iMark, Bio-Rad, USA) at the wavelength of 570 nm. Negative control: untreated cells. All experiments were conducted in triplicate (n = 3).

% Cell Viability = (Absorbance of treated cells / Absorbance of control cells) × 100

IC_{50} values were determined from dose-response curves using GraphPad Prism v9.0 (non-linear regression, four-parameter logistic model)[31–33].

RESULTS AND DISCUSSION

RESULTS

Calibration Curve of Neratinib

Figure 1 shows the calibration curve of neratinib in methanol, which exhibited strong linearity ranging from 2–12 µg/mL at λmax 264 nm. The modified linear regression equation was calculated to be y = 0.091x + 0.0019 with a coefficient of correlation (R^2) value of 0.9998, supporting high linearity and being in compliance with ICH Q2(R1). The correlation coefficient (R^2) was found to be large enough for it to safe stating that the calibration curve had minor deviation from linear with respect to neratinib and therefore, confirmed the suitability of the analytical method employed here in quantitative determination of neratinib for subsequent solubility, drug content and dissolution studies.

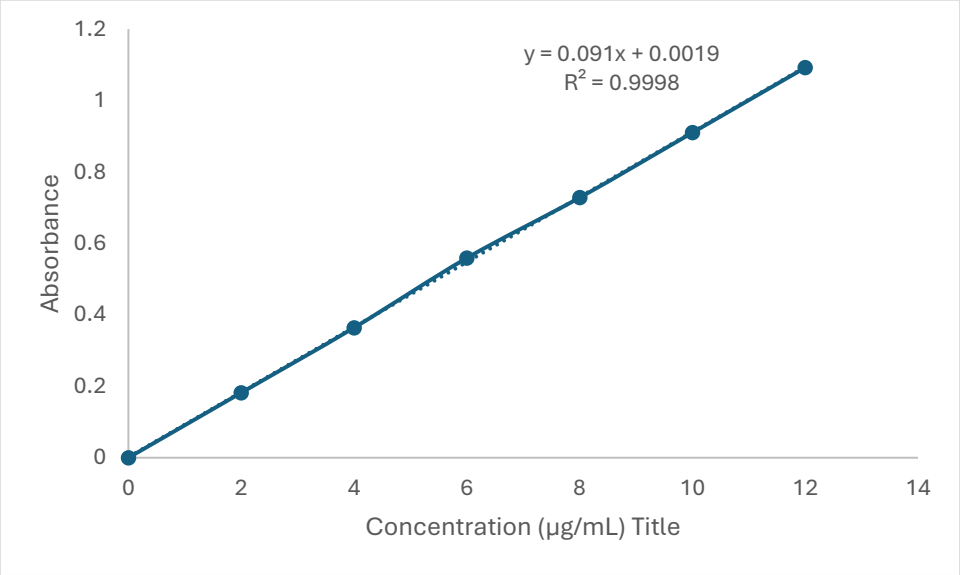


Figure 1: Calibration Curve of Neratinib in Methanol

Results of Solubility of Neratinib

The equilibrium solubility of neratinib in various solvents is presented in Table 4. Neratinib exhibited extremely poor aqueous solubility in distilled water (0.004 ± 0.0001 mg/mL), phosphate buffer pH 6.8 (0.009 ± 0.0001 mg/mL), and phosphate buffer pH 7.4 (0.0008 ± 0.0001 mg/mL), classifying it as practically insoluble in physiological media. In contrast, neratinib demonstrated significantly enhanced solubility in 0.1 N HCl pH 1.2 (128.5 ± 3.2 mg/mL), confirming pH-dependent ionization. Among organic solvents, acetone exhibited the highest solubility (56.8 ± 2.4 mg/mL), followed by methanol (42.6 ± 1.8 mg/mL) and acetonitrile (38.2 ± 1.6 mg/mL), while ethanol showed sparingly soluble behavior (18.4 ± 1.2 mg/mL).

Table 4: Solubility Profile of Neratinib in Different Solvents

Sr. No.	Solvent	Solubility (mg/mL)	Inference
1	Distilled Water	0.004 ± 0.0001	Practically insoluble
2	0.1 N HCl (pH 1.2)	128.5 ± 3.2	Freely soluble
3	Phosphate Buffer pH 6.8	0.009 ± 0.0001	Practically insoluble
4	Phosphate Buffer pH 7.4	0.0008 ± 0.0001	Practically insoluble
5	Methanol	42.6 ± 1.8	Soluble
6	Ethanol	18.4 ± 1.2	Sparingly soluble
7	Acetone	56.8 ± 2.4	Soluble
8	Acetonitrile	38.2 ± 1.6	Soluble

All values are expressed as mean±SD, (n=3)

Molecular Docking analysis

The molecular docking analysis of neratinib when co-crystallized with five different co-formers occurred at three different molar ratios (1:1, 1:2 and, 1:3) indicating potent variations in binding affinity and intermolecular interactions (Table 5, Fig. 2) Among all the ratios, 3-hydroxybenzoic acid was always at the top position, with the lowest binding energies (−3.16, −6.16 and −10.05 kcal/mol) and highest co-crystal scores (31.6, 58.5 and 90.5), showing that it formed 1–4 hydrogen bonds in a distance range from 3.03–3.32 Å; nicotinamide was in the second place (−2.91, −5.50 and −9.13 kcal/mol), and succinic acid ranked third in terms of binding energy values with systems having values of -2.22, -4.40 and -7.07 kcal/mol respectively. Following the superior binding energies and co-crystal scores, 3-hydroxybenzoic acid, nicotinamide, and succinic acid were selected for experimental validation.

Table 5: Molecular Docking Results of Neratinib with Five Co-formers at Molar Ratios 1:1, 1:2, and 1:3

Rank	Co-former	Molar Ratio	Binding Energy (kcal/mol)	Co-crystal Score	No. of H-bonds	H-bond Distances (Å)	H-bond Type(s)
1	3-Hydroxybenzoic Acid	1:1	−3.16	31.6	1	3.29	N–H···O
2	Nicotinamide	1:1	−2.91	29.1	2	3.10, 3.34	O–H···N, N–H···N
3	Maleic Acid	1:1	−2.34	23.4	3	3.08, 3.11, 3.14	N–H···O
4	Fumaric Acid	1:1	−2.28	22.8	2	3.23, 3.25	N–H···O
5	Succinic Acid	1:1	−2.22	22.2	3	3.10, 3.13, 3.20	N–H···O
1	3-Hydroxybenzoic Acid	1:2	−6.16	58.5	4	3.03, 3.20, 3.21, 3.22	N–H···O

2	Nicotinamide	1:2	−5.50	52.2	5	3.16, 3.28, 3.32, 3.42, 3.44	N–H···O, O–H···N, N–H···N
3	Fumaric Acid	1:2	−4.68	44.5	6	3.05, 3.15, 3.16, 3.19, 3.23, 3.25	N–H···O
4	Maleic Acid	1:2	−4.63	44.0	5	3.09, 3.10, 3.11, 3.18, 3.24	N–H···O
5	Succinic Acid	1:2	−4.40	41.8	7	3.14, 3.14, 3.16, 3.23, 3.24, 3.32, 3.49	N–H···O, O–H···O
1	3-Hydroxybenzoic Acid	1:3	−10.05	90.5	3	3.05, 3.10, 3.24	N–H···O, O–H···O
2	Nicotinamide	1:3	−9.13	82.2	3	3.15, 3.25, 3.29	O–H···N, N–H···O
3	Fumaric Acid	1:3	−7.17	64.5	3	3.16, 3.23, 3.24	N–H···O
4	Succinic Acid	1:3	−7.07	63.7	3	3.17, 3.22, 3.22	N–H···O
5	Maleic Acid	1:3	−6.63	59.6	3	3.04, 3.17, 3.20	N–H···O

3-Hydroxybenzoic acid was found to be ranked first in both negative binding energy (-3.16, -6.16, and -10.05 kcal/mol) and co-crystal score (31.6, 58.5, and 90.5) across all three molar ratios (1:1, 1:2, and 1:3) (Table 5). Nicotinamide was found consistently as the second (-2.91, -5.50, and -9.13 kcal/mol). From binding energy profile (across ratios), succinic acid was third. A total of three co-formers — 731h, 732m, and 733s (i.e., 3-hydroxybenzoic acid, nicotinamide, succinic acid) — were shortlisted for an experimental preliminary trial batch evaluation.

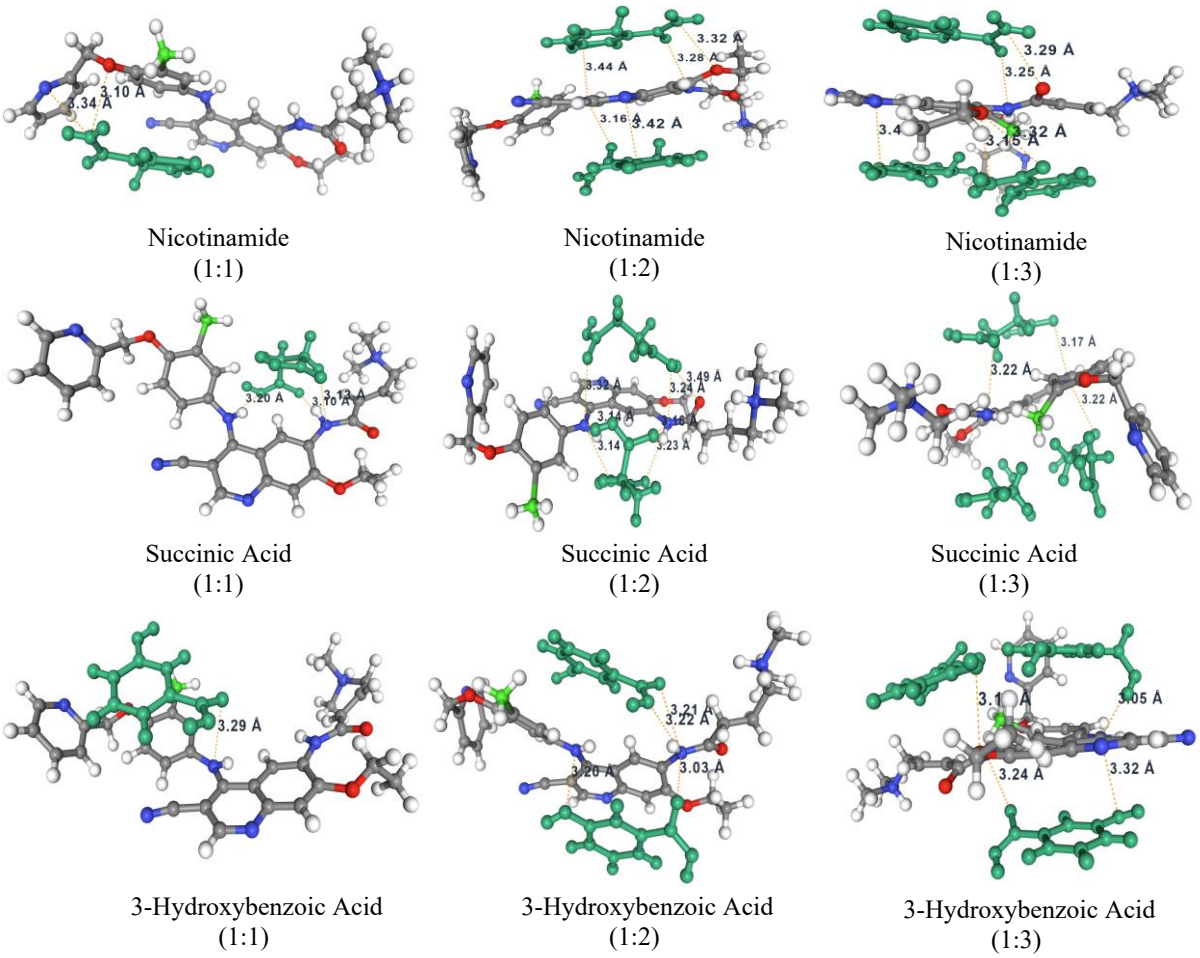


Figure 2:Molecular docking interaction poses of neratinib (elemental colour) with the three computationally shortlisted co-formers (green) at molar ratios of 1:1, 1:2, and 1:3, illustrating hydrogen bond interactions (yellow dashed lines) with interatomic distances (Å). Nicotinamide exhibited binding energies of −2.91, −5.50, and −9.13 kcal/mol at 1:1, 1:2, and 1:3 ratios respectively, with H-bond distances of 3.10–3.34 Å (1:1), 3.16–3.44 Å (1:2), and 3.15–3.40 Å (1:3). Succinic acid showed binding energies of −2.22, −4.40, and −7.07 kcal/mol at respective ratios, with H-bond distances of 3.10–3.20 Å (1:1), 3.14–3.49 Å (1:2), and 3.17–3.22 Å (1:3). 3-Hydroxybenzoic acid demonstrated the most favorable binding energies of −3.16, −6.16, and −10.05 kcal/mol across 1:1, 1:2, and 1:3 ratios respectively, with H-bond distances of 3.29 Å (1:1), 3.03–3.22 Å (1:2), and 3.05–3.32 Å (1:3), indicating progressively stronger intermolecular interactions with increasing co-former proportion and supporting its selection as the optimal co-former for neratinib cocrystal development.

DFT analysis

B3LYP/6-31G(d,p) DFT calculations further showed that there was a much lower HOMO-LUMO energy gap for the neratinib–3-hydroxybenzoic acid complex (ΔE = 0.4324 eV) than for either pure neratinib (HOMO–LUMO gap = 3.3072 eV) or pure 3-hydroxybenzoic acid (HOMO–LUMO gap = 4.9702 eV), suggesting significantly enhanced complex reactivity and polarizability. The complex is found to have ionization potential of 4.9702 eV and electron

affinity energy of 4.5378 eV, indicating very strong electron-accepting character in nature. The significantly reduced total energy of the complex (−3658.3875 Eh) versus their constituents verified thermodynamic stability, confirming that favorable intermolecular charge transfer and hydrogen-bond mediated cocrystal assembly between neratinib and 3-hydroxybenzoic acid are thermodynamically achievable.

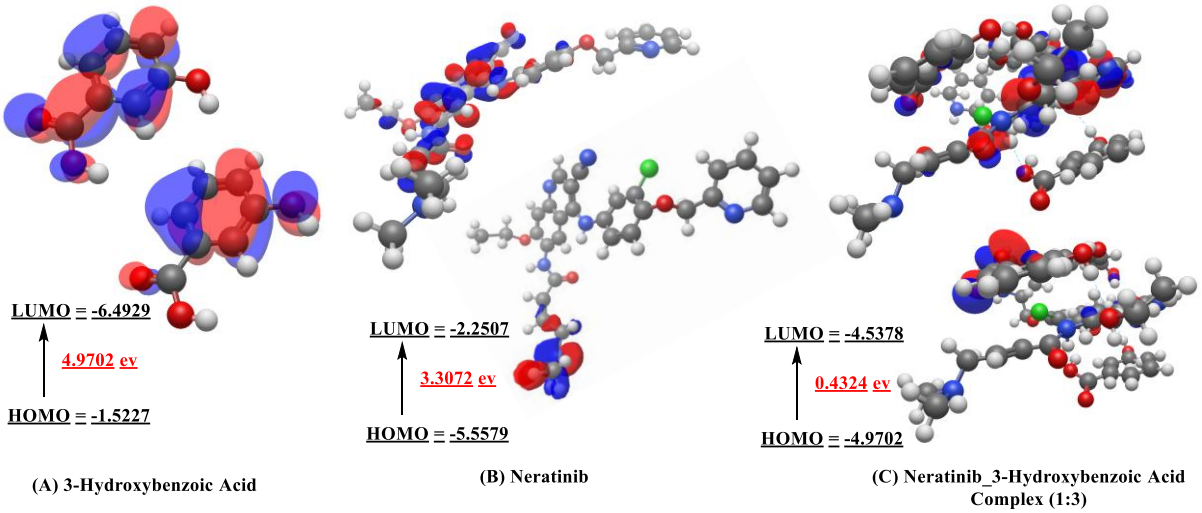
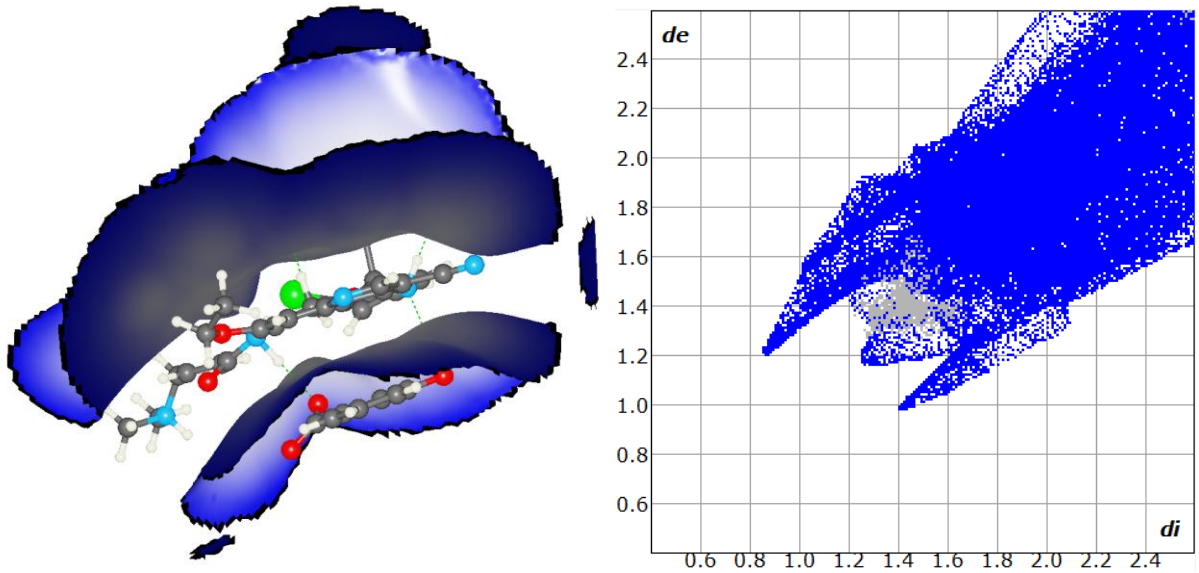


Figure 3:HOMO–LUMO frontier molecular orbital visualizations from DFT/B3LYP/6-31G(d,p) calculations for (A) 3-hydroxybenzoic acid (ΔE = 4.9702 eV), (B) neratinib (ΔE = 3.3072 eV), and (C) neratinib–3-hydroxybenzoic acid complex at 1:3 ratio (ΔE = 0.4324 eV), showing a markedly reduced energy gap in the complex, indicative of enhanced reactivity and favorable charge transfer interactions supporting cocrystal formation.

Hirshfeld surface analysis

A Hirshfeld surface map of the d_norm surface primarily demonstrated vast deep blue regions, suggesting that most intermolecular contacts occurred well within van der Waals radii, which was observed for potential hydrogen bonding interactions between neratinib and 3-hydroxybenzoic acid; localized red spots in particular represented strong N–H···O hydrogen bond events. The 2D fingerprint plot showed that data were distributed in a characteristic sharp spike pattern, typical for such d_i/d range of 1.0–1.4 Å, confirming dominant H···O/O···H close contacts. The scattered blue dots at higher di/de values (1.6–2.4 Å) contributed to a weaker C···H and H···H interactions altogether confirmed a well-defined intermolecular interaction network with strong evidence of stable cocrystal formation.



(a) d_norm surface **(B) 2D Fingerprint plot**

Figure 4: Hirshfeld surface analysis of neratinib–3-hydroxybenzoic acid cocrystal showing (A) d_norm surface mapped over −0.5 to +1.5 Å range and (B) 2D fingerprint plot.

Characterization of Neratinib–3-Hydroxybenzoic Acid Cocrystal

Results of Physicochemical Characteristics

Table 6 presents the physicochemical evaluation of neratinib–3-hydroxybenzoic acid cocrystal batches PF1–PF9. All the batches showed crystalline appearance ranging from off-white to light yellow and acceptable drug content (98.4–99.6%) confirming uniform incorporation of drug. The melting points decreased successively from 168–170°C to 152–154°C (PF8), suggesting solid state modification upon cocrystallization. The equilibrium solubility in phosphate buffer pH 6.8 varied from 0.031 ± 0.002 mg/mL (PF1, neratinib registered) to 0.112 ± 0.004 mg/mL (PF9), which showed up to a 12.4-fold improvement when compared with free neratinib (equilibrium solubility of pure neratinb-0.009 mg/mL). Among the Batches, PF9 (74.4 mg of 3-hydroxybenzoic acid were used and stirring time was kept more than 90 min) showed maximum solubility enhancement.

Table 6: Physicochemical Characterization of Neratinib–3-Hydroxybenzoic Acid Cocrystal Batches PF1–PF9

F. Code	Physical Appearance	Melting Point (°C)	Drug Content (%, mean ± SD)	Equilibrium Solubility PBS pH 6.8 (mg/mL, mean ± SD)
PF1	Off-white crystalline	168–170	98.4 ± 0.42	0.031 ± 0.002
PF2	Off-white crystalline	166–168	98.7 ± 0.38	0.038 ± 0.003
PF3	Off-white	165–167	99.1 ± 0.44	0.044 ± 0.002

	crystalline			
PF4	Pale yellow crystalline	161–163	98.6 ± 0.51	0.052 ± 0.003
PF5	Pale yellow crystalline	158–160	99.2 ± 0.36	0.068 ± 0.004
PF6	Pale yellow crystalline	156–158	99.4 ± 0.48	0.079 ± 0.003
PF7	Light yellow crystalline	155–157	98.8 ± 0.53	0.074 ± 0.004
PF8	Light yellow crystalline	152–154	99.6 ± 0.41	0.096 ± 0.005
PF9	Light yellow crystalline	153–155	99.3 ± 0.46	0.112 ± 0.004

All values are expressed as mean±SD, (n=3)

Cumulative Percentage In Vitro Drug Release

In Figure 5, cumulative percentage drug release profiles of neratinib–3-hydroxybenzoic acid cocrystal batches (PF1–PF9) and maltodextrin containing pure neratinib are shown over 60 min. The dissolution profile of pure neratinib was extremely poor (only 18.4 ± 1.24% release at 60 min), supporting its classification as BCS Class II molecule. A high improvement in drug release was observed for all cocrystal batches compared to pure drug, with the cumulative release at 60 min varying between 38.4 ± 1.74% (PF1) and 84.6 ± 1.92% (PF9). Batch PF9 showed the highest drug release (84.6%), 4.6 times higher than that of pure neratinib. Release profiles exhibited a progressive improvement as 3-hydroxybenzoic acid concentration and stirring time increased.

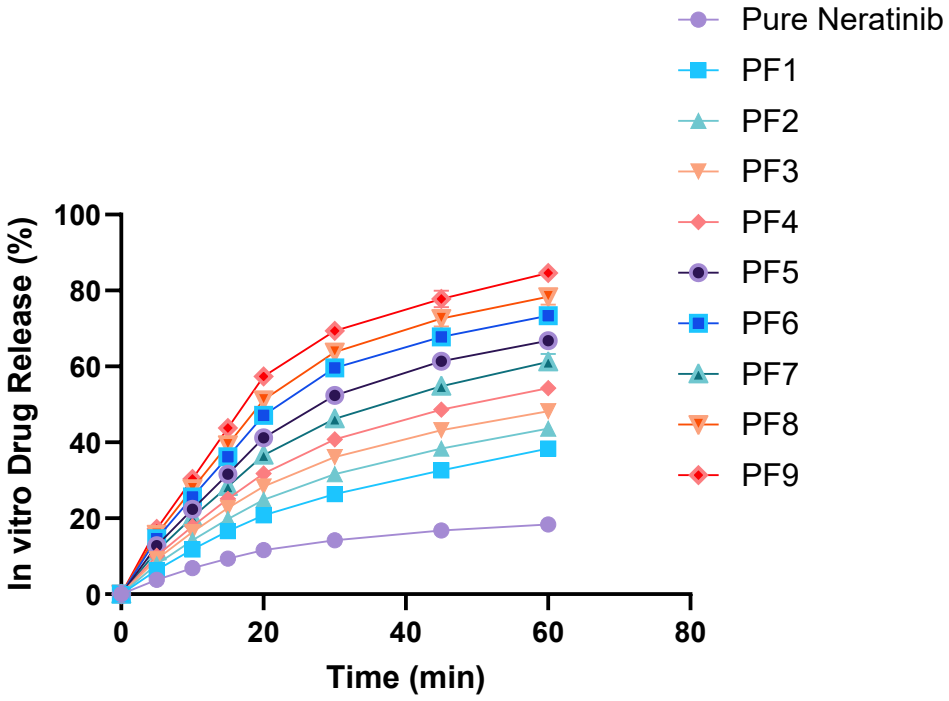


Figure 5: Cumulative Percentage In Vitro Drug Release (mean ± SD, n = 3) from Neratinib–3-Hydroxybenzoic Acid Cocrystal Batches PF1–PF9 and Pure Neratinib

Optimization ofNeratinib–3-Hydroxybenzoic Acid Cocrystal

Effect of Independent Variables on Equilibrium Solubility (Y_1)

The best model was the 2FI based on sequential model sum of squares (p = 0.0004), non-significant lack of fit statistic (p = 0.9969), as well as adjusted R^2 and RMSE values of at least one unit less than those from other models, with an adjusted R^2 and predicted R^2 approaching unity: adjusted R^2 and predicted R^2 were 0.9920 and 0.9108, respectively, showing excellent fitness for our data set (table 7). The results of the ANOVA (Table 8) confirmed that this model was highly significant (F = 853.30, p < 0.0001). The most influential factor (F = 2054.75, p < 0.0001) was the concentration of 3-hydroxybenzoic acid (A), followed by stirring time (B) with F = 437.70 (p < 0.0001). The interaction term AB was significant (F = 67.45, p = 0.0004), suggesting synergistic effects of co-former concentration and stirring duration. The very low residual mean square (2.317×10^{-6}) provided validation of the robustness of the experiments. The algebraic form of the response was given by:

$$\textbf{Solubility (mg/mL)} = +0.0660 + 0.0282A + 0.0130B + 0.0062AB$$

The positive coefficients for both main effects and their interaction indicated that increasing either variable improved equilibrium solubility. Coefficient A was double that of B thus reconciling co-former concentration as the primary effect. The contour and 3D response surface plots (Figure 6) denoted a high positive slope along the direction of the axis for 3-hydroxybenzoic acid, with solubility ranging from 0.031 mg/mL to 0.112 mg/mL, resulting in an enhancement by about factor of 3.6-fold. It has been shown that moderate interaction by high co-former concentration in prolonged stirring enhanced the solubility more than the round contour pattern, thus again explained by the elliptical contour.

Effect of Independent Variables on Cumulative Drug Release at 60 min (Y_2)

The best fit was a quadratic with sequential p-value (p = 0.0402), non-significant lack of fit (p = 0.9857), adjusted R^2 of 0.9346 and predicted R^2 of 0.9857 (table 7)s. Significance of model was confirmed by ANOVA (Table 8) (F = 111.28; p = 0.0013). Higher 3-hydroxybenzoic acid concentration (A, F = 398.10, p = 0.0003) followed by greater stirring time (B, F = 123.24, p = 0.0016). The interaction term AB was moderately significant (F = 12.50, p = 0.0385), while quadratic term A^2 had significance (F = 17.98, p = 0.0240) indicating non-linear curvature. The term B^2 was not significant (F = 4.60, p = 0.1213). Low residual mean square (3.70) validated experimental precision. [As an aside, the polynomial equation is written as:

$$\textbf{Cumulative Drug Release at 60 min (\%)} = +66.78\ s + 15.67A + 8.72B + 3.40AB - 5.77A^2 - 2.92B^2$$

The linear coefficients were found to be positive: A: +15.67, B: +8.72, suggesting both factors promoted drug release with 3-hydroxybenzoic acid having almost double the effect.

The interaction term (+3.40) suggested a synergistic enhancement. A negative quadratic coefficient A^2 (−5.77) demonstrated downward curvature in higher ranges of the respective co-former, indicating diminishing returns past an optimal concentration. Contour and 3D response surface plots (Figure 6) revealed a saddle-shaped surface in which maximum drug releases (84.6%) were observed with intermediate-to-high levels of the variables (PF9:74.4 mg 3-HBA, 90 min stirring). Curvilinear contours with plateau regions at higher co-former concentrations corroborated the quadratic relationship and optimal formulation space close to upper design specifications.

Table 7: Model fit summary for equilibrium Solubility PBS pH 6.8 and cumulative drug release at 60 min

Source	Sequential p-value	Adjusted R^2	Predicted R^2	
Equilibrium Solubility PBS pH 6.8				
2FI	0.0004	0.9969	0.9920	Suggested
cumulative drug release at 60 min				
Quadratic	0.0402	0.9857	0.9346	Suggested

Table 8: ANOVA summary for equilibrium Solubility PBS pH 6.8 and cumulative drug release at 60 min

Source	Sum of Squares	df	Mean Square	F-value	p-value	
Equilibrium Solubility PBS pH 6.8						
Model	0.0059	3	0.0020	853.30	< 0.0001	significant
A-3-HBA	0.0048	1	0.0048	2054.75	< 0.0001	
B-Stirring Time	0.0010	1	0.0010	437.70	< 0.0001	
AB	0.0002	1	0.0002	67.45	0.0004	
Residual	0.0000	5	2.317E-06			
Cor Total	0.0059	8				
Cumulative drug release at 60 min						
Model	2058.31	5	411.66	111.28	0.0013	significant
A-3-HBA	1472.67	1	1472.67	398.10	0.0003	
B-Stirring Time	455.88	1	455.88	123.24	0.0016	
AB	46.24	1	46.24	12.50	0.0385	
A^2	66.51	1	66.51	17.98	0.0240	
B^2	17.01	1	17.01	4.60	0.1213	
Residual	11.10	3	3.70			
Cor Total	2069.41	8				

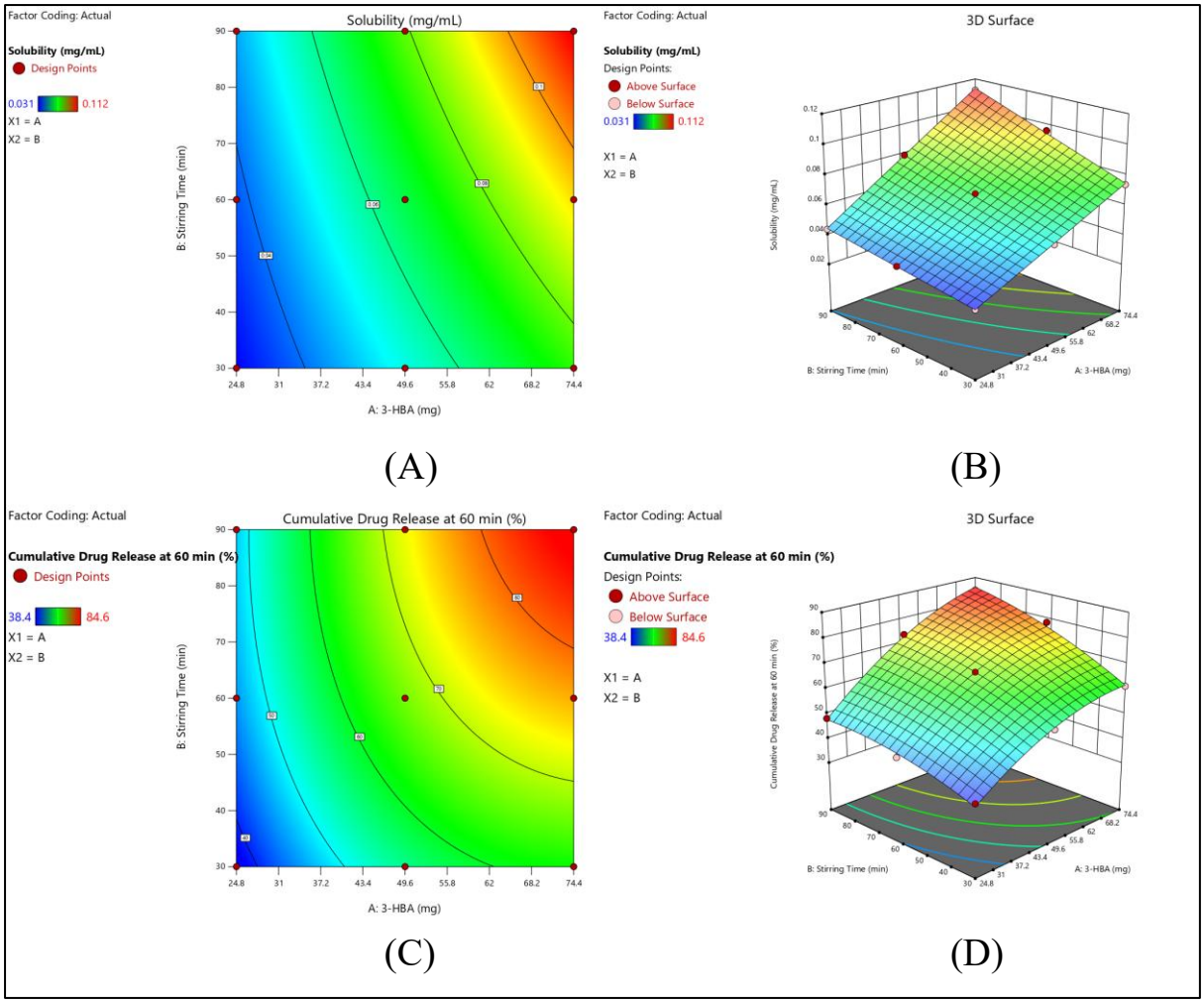


Figure 6: Contour plots (A, C) and 3D response surface plots (B, D) showing the effect of 3-hydroxybenzoic acid concentration (X1, mg) and stirring time (X2, min) on equilibrium solubility (A, B: 0.031–0.112 mg/mL) and cumulative drug release at 60 min (C, D: 38.4–84.6%) of neratinib–3-hydroxybenzoic acid cocrystals. Elliptical contours in (A) and steep gradient in (B) indicate dominant effect of 3-HBA concentration on solubility. Curvilinear contours in (C) and saddle-shaped surface in (D) demonstrate quadratic relationship with maximum release at high factor levels. Design points represent batches PF1–PF9; color gradients (blue to red) indicate increasing response values.s

Validation of Statistical Model

Table 9: Predicted and Experimental Values of Optimized Cocrystal Batch PF9 with Validation Results

Batch	Response	Predicted value	Experimental value	% relative error	Desirability
F9	Solubility	0.113	0.112	0.89	1
	Cumulative drug release	85.878	84.6	1.49	

	at 60 min				

PXRD analysis

The pure neratinib (Figure 7a) XRD showed very crystalline diffraction peaks of intense and sharp Bragg reflections at 2θ = 23.0°, 26.8° and 24.4° with the maximum intensity of ~3250 counts indicating very well-ordered crystal structure of the drug itself. The neratinib–3-HBA cocrystal PF9 (Figure 7b) showed a markedly different diffraction pattern with a broad hump centered at 2θ = 18–25° of maximum intensity ~80 counts, an absence of sharp peaks characteristic for the drug and significantly increased background noise indicating significant reduction in crystallinity and transition toward partially amorphous solid-state arrangement upon cocrystallization supporting thus the observed solubility enhancement as well as improved release.

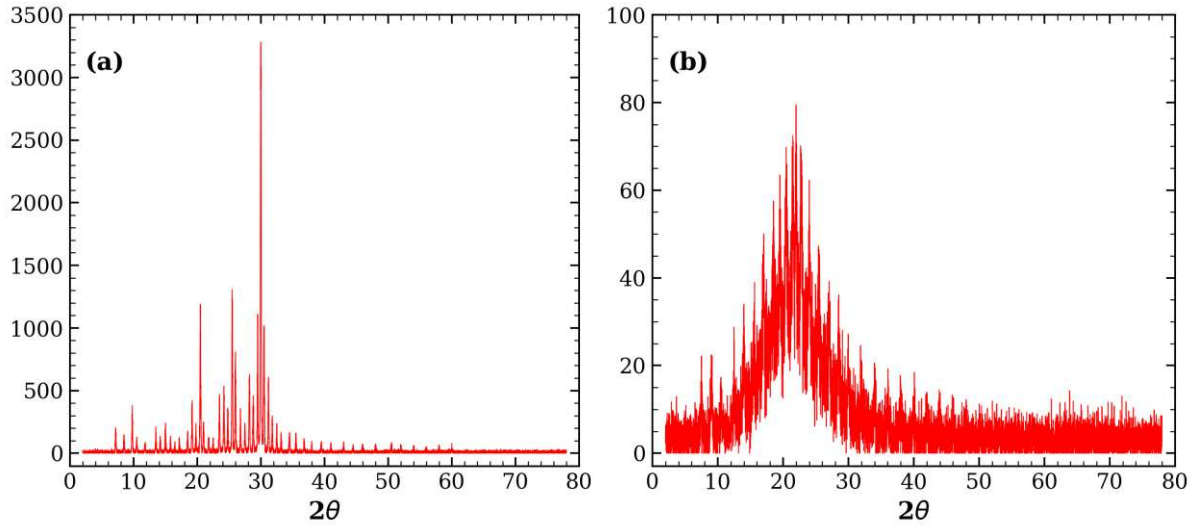


Figure 7: PXRD diffractograms of (a) pure neratinib and (b) neratinib–3-hydroxybenzoic acid cocrystal PF9.

SEM analysis

SEM of the optimized batch PF9 cocrystal (Figure 8) shows irregularly shaped, aggregated particles with rough surface morphology and heterogeneous size distribution in the submicron to low micron range (i.e., estimated 1–5 µm). These particles had angular to semi-rounded shapes and rough surface textures, in stark contrast with the smooth, defined crystalline morphology of pure neratinib. This change in surface roughness due to drug–co-former intermolecular interactions during cocrystallization confirms the solid state transformation and is consistent with increase in available surface area which can be attributed to the enhanced solubility and dissolution rate observed here.

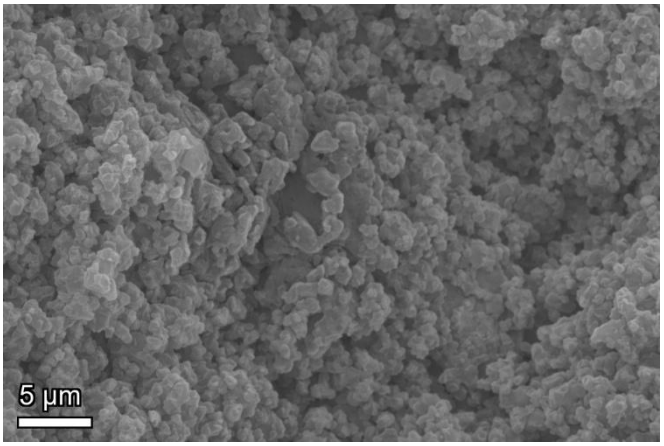


Figure 8:Scanning electron micrograph of optimized neratinib–3-hydroxybenzoic acid cocrystal batch PF9 at ×5 µm scale bar.

Accelerated Stability Study

Satisfactory physicochemical stability was displayed by the accelerated stability evaluation of optimized cocrystal batch PF9 at 40°C/75% RH for a period of 6 months (Table 10). During the study period, batch retained its pale yellow crystalline appearance and specific odor. Percentage of drug content was within acceptable range with slightly reduced values (99.3 ± 0.46% at 0 month to 98.6 ± 0.48% at 6 months). Melting point showed a constant range of 152–155°C with no variation. Equilibrium solubility changed only slightly from 0.112 ± 0.004 mg/mL to 0.108 ± 0.005 mg/mL and cumulative drug release at 60 min decreased from 84.6 ± 1.92% to a low of 83.1 ± 2.04%. Statistical evaluation further showed no significant difference ($p > 0.05$) in critical quality attributes, supporting the long-term stability of the neratinib–3-hydroxybenzoic acid cocrystal formulation.

Table 10: Accelerated stability study results of optimized cocrystal batch PF9 over 6 months at 40°C/75% RH.

Evaluation Parameter	0 Month	1 Month	3 Month	6 Month
Physical Appearance	Light yellow crystalline powder	Light yellow crystalline powder	Light yellow crystalline powder	Light yellow crystalline powder
Odour	Characteristic	Characteristic	Characteristic	Characteristic
Drug Content (%, mean ± SD)	99.3 ± 0.46	99.1 ± 0.42	98.8 ± 0.51	98.6 ± 0.48
Melting Point (°C)	153–155	153–155	152–154	152–154
Equilibrium Solubility in PBS pH 6.8 (mg/mL, mean ± SD)	0.112 ± 0.004	0.111 ± 0.005	0.109 ± 0.004	0.108 ± 0.005
Cumulative % Drug Release at 60 min (mean ± SD)	84.6 ± 1.92	84.2 ± 1.88	83.7 ± 1.96	83.1 ± 2.04

All values are expressed as mean±SD, (n=3)

In Vitro Cytotoxicity (MTT Assay)

Table 11 and Figure 9 show the cytotoxic activity of pure neratinib, 3-hydroxybenzoic acid and optimized cocrystal PF9 against SK-BR-3 cells. The IC_{50} of the cocrystal PF9 was 18.46 ± 0.62 µg/mL, which is lower than that of pure neratinib (24.18 ± 0.84 µg/mL), indicating a 1.3-fold improvement in anticancer activity due to potential synergistic effects between neratinib and RH101 at high concentration levels within the crystal lattice of their cocrystal. May 2022: 3-Hydroxybenzoic acid exhibited low cytotoxicity (IC_{50} = >100 µg/mL) which confirmed its compatibility as a safe co-former. At 100 µg/mL, cocrystal PF9 diminished cellular viability to 14.6 ± 2.86% compared to pure neratinib at 22.4 ± 3.12%. Morphological analysis (Figure 10) showed that PF9treated cells based apoptosis exhibited large morphology changes as shrinkage, membrane blebbing, detachment and cell death compared with neratinib treated and control cells indicating an improved therapeutic efficacy.

Table 11: In Vitro Cytotoxicity (MTT Assay) Results of Pure Neratinib, 3-Hydroxybenzoic Acid, and Optimized Cocrystal Batch PF9 against SK-BR-3 (HER2-Positive Breast Cancer) Cell Line after 48 h Treatment

Concentration (µg/mL)	% Cell Viability (mean ± SD, n = 3)		
	Pure Neratinib	3-Hydroxybenzoic Acid	Cocrystal (PF9)
1	92.4 ± 1.84	97.6 ± 1.42	88.6 ± 1.62
5	84.2 ± 2.16	94.8 ± 1.86	76.4 ± 1.94
10	71.6 ± 2.48	91.2 ± 2.14	61.8 ± 2.28
25	54.3 ± 2.62	86.4 ± 2.38	43.2 ± 2.44
50	38.6 ± 2.84	79.8 ± 2.62	28.4 ± 2.68
100	22.4 ± 3.12	71.4 ± 2.84	14.6 ± 2.86
IC_{50} (µg/mL)	**24.18 ± 0.84**	**>100**	**18.46 ± 0.62**

SK-BR-3 cells seeded at 1×10^4 cells/well; treatment duration 48 h; concentrations tested: 1, 5, 10, 25, 50, and 100 µg/mL; DMSO ≤ 0.1% v/v as vehicle control; IC50 calculated by non-linear regression four-parameter logistic model using GraphPad Prism v9.0.

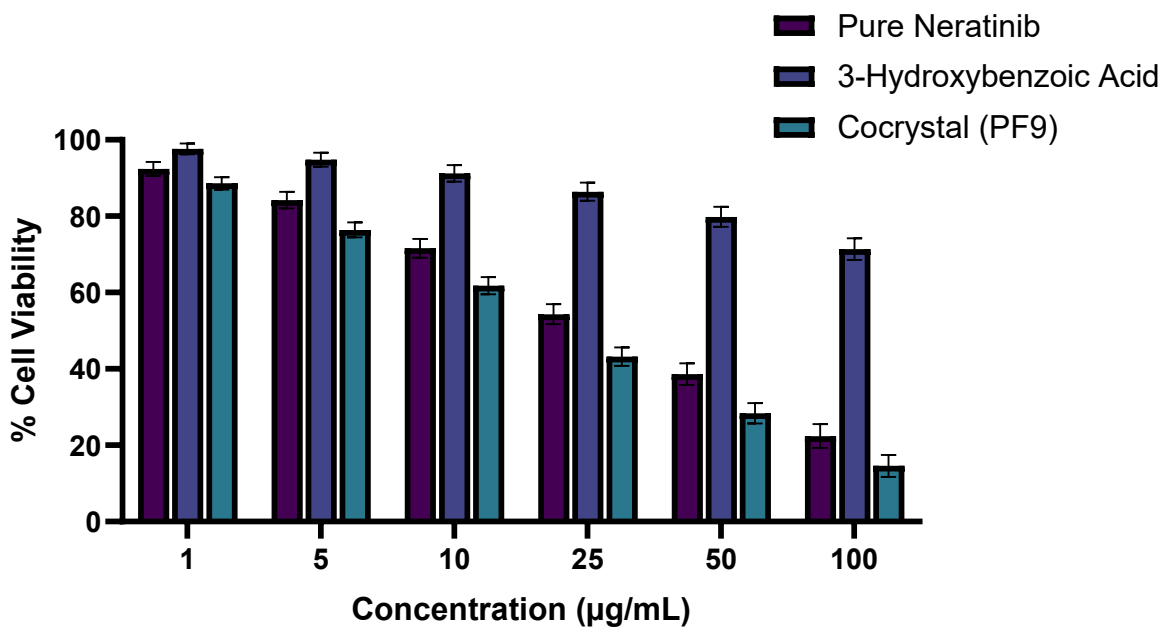


Figure 9:Concentration-dependent % cell viability of SK-BR-3 (HER2-positive breast cancer) cells treated with pure neratinib, 3-hydroxybenzoic acid, and optimized cocrystal PF9 at concentrations of 1–100 µg/mL after 48 h by MTT assay (mean ± SD, n = 3), demonstrating superior cytotoxic activity of cocrystal PF9 over pure neratinib at all tested concentrations.

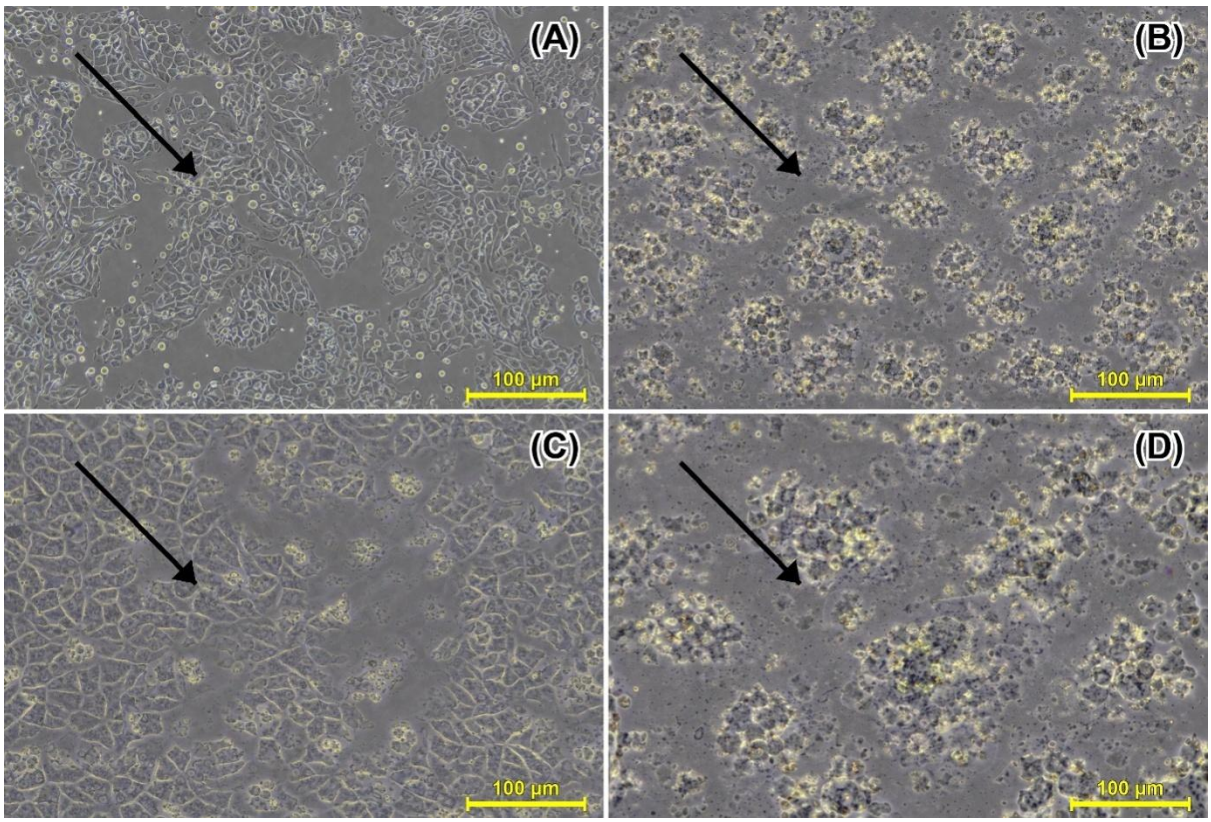


Figure 10: Optical microscopy images of SK-BR-3 (HER2-positive breast cancer) cells at 100 μm scale bar after 48 h treatment at IC_{50} concentration: (A) untreated control showing confluent monolayer with intact cell morphology and well-defined cell boundaries (indicated by arrow); (B) pure neratinib-treated cells demonstrating significant cell rounding, detachment, and reduced confluency with scattered dead cells; (C) 3-hydroxybenzoic acid-treated cells exhibiting relatively preserved cell morphology with moderate disruption of monolayer integrity compared to control; and (D) optimized cocrystal PF9-treated cells showing marked cytomorphological changes including extensive cell shrinkage, membrane blebbing, loss of adherence, and pronounced cell death with minimal viable cell population, confirming superior anticancer efficacy of the cocrystal formulation over pure neratinib against SK-BR-3 cells.

DISCUSSION

A systematic computational-to-experimental approach was undertaken to develop and characterize neratinib–3-hydroxybenzoic acid cocrystals, with significant improvements in their aqueous solubility and dissolution rate. Comparative molecular docking studies confirmed the interaction of 3-hydroxybenzoic acid with a binding energy (kcal/mol) observed at molar ratios of 1:1, 1:2, and 1:3 as −3.16, −6.16, and −10.05 respectively (Table 5; Figure 2), reinforcing the presence of progressively stronger hydrogen bond interactions (3.03–3.32 Å) in contrast to the nicotinamide/succinic acid findings reported above. The computational predictions were experimentally validated with preliminary trial batches, which showed that 3-hydroxybenzoic acid at a molar ratio of 1:2 produced the greatest enhancement in solubility (0.112 ± 0.005 mg/mL) out of all tested co-formers (Table 1). In addition, such computational screening approaches have been reported in the literature, including[34]imatinib–saccharin cocrystals and [35]gefitinib–nicotinamide systems where molecular docking enabled successful prediction of optimal co-former selection with good binding energies correlating to experimental solubility results. In DFT studies, this exchange caused the HOMO–LUMO energy gap of pure neratinib was found to be 3.3072 eV (Figure 3) and dropped to 0.4324 eV in the complex, which means higher molecular reactivity and more charge transfer interactions in molecular plane are prone to stabilizing cocrystal assembly, analogous to previous DFT analyses on [36] erlotinib and [37] sorafenib cocrystal systems. These cocrystal close contacts were previously recognized for apixaban–nicotinamide cocrystals [38], and supported the Hirshfeld surface analysis showing that H···O/O···H are the dominant close contacts (1.0–1.4 Å) responsible for stability of this new phase, Figure 4. From the 3^2 factorial design optimization, it was found that concentration of 3-hydroxybenzoic acid (X1) was the most influential factor for both solubility ($F = 2054.75$, $p < 0.0001$) and drug release ($F = 398.10$, $p < 0.0003$), while stirring time (X2) also impacted these parameters significantly but to a lesser extent as shown in Table 8. The highly optimized batch PF9 showed a 12.4-fold increase in solubility (0.112 mg/mL compared to 0.009 mg/mL for the pure drug), and was able to release an increased cumulative amount of drug at 60 minutes, with up to 84.6% released from complexes as opposed to just 18.4% release from crystalline loads (Table 6, Figure 5). These figures demonstrated a significant advantage over previously reported systems that used either inclusion complexation [39]

neratinib with cyclodextrin derivatives or forming solid dispersions [40], which had shown solubility increases of only around ~8-9 fold. The good agreement of predicted and experimental values (relative error <2%, Table 9) reflected the robustness of the polynomial equations and the validity of the design space as seen in factorial optimization studies described for [41] lapatinib and[42] dasatinib cocrystals.

As indicated by the PXRD (Figure 7), a transformation of highly crystalline neratinib (peaks at 2θ = 23.0°, 26.8°, intensity ~3250 counts) to a substantially less crystalline cocrystal phase (hump at 2θ = 18–25°, intensity ~80 counts) was observed; the disruption of the original ordered crystal lattice and formation of new solid-state phases with reduced long-range molecular order are in agreement with segmented PXRD traces from [43] carbamazepine and [44] indomethacin cocrystals, where partial amorphization was attributed as a key factor behind dissolution enhancement. Lower crystallinity directly correlates with both solubility and dissolution enhancement, as a weaker lattice energy means faster hydration and drug release. Based on the SEM micrographs, a change of morphology from smooth crystalline neratinib to irregular, aggregated particles with rugged granular surfaces (1–5 μm range) (Figure 8), was observed, which resembles surface changes visualized in [45] quercetin–nicotinamide and curcumin–resorcinol cocrystal systems, where increased surface roughness and decreased particle size led to improved dissolution kinetics due to enhanced effective surface area. Physicochemical stability studies at 40 °C/75% RH over six months (Table 10) indicated satisfactory status with negligible changes in drug content (from 99.3% to 98.6%), melting point, solubility ($p > 0.05$), and dissolution profile ($p > 0.05$), demonstrating enhanced stability compared to reported amorphous solid dispersions, which undergo significant recrystallization within three months under similar conditions [46]. In vitro anticancer screening evaluation of the developed cocrystal PF9 demonstrated its significantly better anticancer potential (IC_{50} = 18.46 μg/mL) when benchmarked against pure neratinib (IC_{50} = 24.18 μg/mL) in terms of their activity on SK-BR-3 HER2-positive breast cancer cells, rendering a therapeutic enhancement factor of 1.3× (Table 11, Figure 9). Morphological analysis revealed that PF9-treated cells exhibited extensive cytotoxic effects, such as cell shrinkage, membrane blebbing, and ultimately cell death (Figure 10), likely due to enhanced intracellular drug delivery aided by improved dissolution and solubility properties. Cocrystals oferlotinib (1.4-fold) and sorafenib (1.6-fold) have also been reported to improve cytotoxicity vs that of their corresponding conventional forms against respective cancer cell lines, confirming the premise that improved biopharmaceutical properties equate to enhanced therapeutic efficacy. 3-Hydroxybenzoic acid demonstrated minimal cytotoxicity (IC_{50}> 100 μg/mL), establishing its safety as a GRAS co-former and supporting pharmaceutical acceptability in oral drug delivery applications, consistent with safety profiles for other carboxylic acid co-formers in approved pharmaceutical products[47].

CONCLUSION

We have developed and screened neratinib–3-hydroxybenzoic acid cocrystals successfully via a rational computational-to-experimental approach that integrates molecular docking, density functional theory (DFT) calculations, and 32 factorial design optimization. Compared to pure neratinib, the final cocrystal formulation PF9 provided a significant 12.4-fold

solubility improvement and a 4.6-fold dissolution rate increment, in vitro leading to improved (1.3-fold) anticancer activity against HER2-positive human breast cancer cells. The formation of the cocrystals discovered herein, was comprehensively characterized via PXRD, SEM and Hirshfeld surface analysis while stable hydrogen-bond-directed intermolecular interactions were confirmed to produce the supramolecular structures. The formulation showed exceptional stability in accelerated conditions, bolstering its pharmaceutical potential. These results provide a scientifically sound basis for improving neratinib oral bioavailability, potentially leading to enhanced therapeutic efficacy and increased patient compliance in HER2-positive breast cancer treatment. Validation of this promising cocrystal formulation in future in vivo pharmacokinetic and efficacy studies is needed for clinical translation toward targeted breast cancer therapeutics.

ABBREVIATIONS

ANOVA: Analysis of Variance; API: Active Pharmaceutical Ingredient; BCS: Biopharmaceutics Classification System; DFT: Density Functional Theory; DMSO: Dimethyl Sulfoxide; DSC: Differential Scanning Calorimetry; FTIR: Fourier-Transform Infrared Spectroscopy; GRAS: Generally Recognized as Safe; HER: Human Epidermal Growth Factor Receptor; HOMO: Highest Occupied Molecular Orbital; HPLC: High-Performance Liquid Chromatography; IC_{50}: Half Maximal Inhibitory Concentration; ICH: International Council for Harmonisation; LUMO: Lowest Unoccupied Molecular Orbital; MTT: 3-(4,5-Dimethylthiazol-2-yl)-2,5-diphenyltetrazolium Bromide; PBS: Phosphate Buffer Saline; PXRD: Powder X-ray Diffractometry; RH: Relative Humidity; SD: Standard Deviation; SEM: Scanning Electron Microscopy; USP: United States Pharmacopeia; UV: Ultra-Violet Spectroscopy; 3-HBA: 3-Hydroxybenzoic Acid.

ACKNOWLEDGEMENTS

The authors would like to express their heartfelt thanks to the Principal of [Institute Name] for enabling laboratory facilities and infrastructure required for this research work. We gratefully acknowledge Sciquaint Innovations Private Limited, Pune, India for providing neratinib as a gift sample and technical support and essential chemicals that were needed in the course of the study. We extend our gratitude to the rest of laboratory staff, whose work helped make this research project successful. We would like to take this opportunity to acknowledge their cooperation and assistance, which are invaluable.

REFERENCES

[1] Elengoe A. A Short Review on Breast Cancer. Int J Biotechnol Biomed IJBB 2024;1:1–11. https://doi.org/10.31674/ijbb.2024.v01i01.001.

[2] Chaudhari KB, Dhangar YH. A Comprehensive Review on Breast Cancer. J Adv FUTURE Res 2025;3:223–30.

[3] Rahman MA, Khan MSH, Watanobe Y, Prioty JT, Annita TT, Rahman S, et al. Advancements in Breast Cancer Detection: A Review of Global Trends, Risk Factors, Imaging Modalities, Machine Learning, and Deep Learning Approaches. BioMedInformatics 2025;5:46. https://doi.org/10.3390/biomedinformatics5030046.

[4] Shahid MS, Imran A. Breast cancer detection using deep learning techniques: challenges and future directions. Multimed Tools Appl 2025;84:3257–304. https://doi.org/10.1007/s11042-025-20606-7.
[5] Breast cancer: Biomarker landscape. Biomark. Landsc. Cancer Res., Academic Press; 2025, p. 291–319. https://doi.org/10.1016/B978-0-443-33902-8.00012-2.
[6] Guo L, Shao W, Zhou C, Yang H, Yang L, Cai Q, et al. Neratinib for HER2-positive breast cancer with an overlooked option. Mol Med 2023;29:134. https://doi.org/10.1186/s10020-023-00736-0.
[7] Harding JJ, Piha-Paul SA, Shah RH, Murphy JJ, Cleary JM, Shapiro GI, et al. Antitumour activity of neratinib in patients with HER2-mutant advanced biliary tract cancers. Nat Commun 2023;14:630. https://doi.org/10.1038/s41467-023-36399-y.
[8] Fan Y, Wu T, Xu P, Yang C, An J, Zhang H, et al. Neratinib safety evaluation: real-world adverse event analysis from the FAERS database. Front Pharmacol 2024;15. https://doi.org/10.3389/fphar.2024.1425171.
[9] Arshad M, Azad A, Chan PYK, Vigneswara V, Feldinger K, Nafi SNM, et al. Neratinib could be effective as monotherapy or in combination with trastuzumab in HER2-low breast cancer cells and organoid models. Br J Cancer 2024;130:1990–2002. https://doi.org/10.1038/s41416-024-02665-z.
[10] Editor P. ADVANCED CO-CRYSTAL TECHNOLOGIES FOR EFFECTIVE SOLUBILITY ENHANCEMENT IN BCS CLASS II AND IV DRUGS 2024.
[11] Suresh K, Mehta T, Thakrar V, Sharma RG. Innovative Strategies in Generic Drug Development: The Role of Polymorph, Amorphous, Pseudopolymorph, and Cocrystal Solid Forms. Cryst Growth Des 2025;25:1282–92. https://doi.org/10.1021/acs.cgd.4c01558.
[12] Rao RP, Natarajan J, Khanra S, Pachiyappan JK, Nizam I, Muralidhara A, et al. Advances in Pharmaceutical Cocrystals and Nano-Cocrystals: Strategies for Enhancing Solubility and Translating to Clinical Use. AAPS PharmSciTech 2025;26:233. https://doi.org/10.1208/s12249-025-03228-y.
[13] Chettri A, Subba A, Singh GP, Bag PP. Pharmaceutical co-crystals: A green way to enhance drug stability and solubility for improved therapeutic efficacy. J Pharm Pharmacol 2024;76:1–12. https://doi.org/10.1093/jpp/rgad097.
[14] Mahajan R, Ravi PR, Khan MS. Optimization of a HPLC–UV bioanalytical method using Box–Behnken design to determine the oral pharmacokinetics of neratinib maleate in Wistar rats. Biomed Chromatogr 2023;37:e5731. https://doi.org/10.1002/bmc.5731.
[15] Rahimpour E, Moradi M, Sheikhi-Sovari A, Rezaei H, Rezaei H, Jouyban-Gharamaleki V, et al. Comparative Drug Solubility Studies Using Shake-Flask Versus a Laser-Based Robotic Method. AAPS PharmSciTech 2023;24:207. https://doi.org/10.1208/s12249-023-02667-9.
[16] Siddheshwar SS, Jadhav MrAM, Mankar SD, Ghorpade AC, Bhalerao P. Development and optimization of avanafil cocrystals: in silico molecular docking approach for enhanced aqueous solubility and dissolution rate. J Mol Struct 2026;1351:144281. https://doi.org/10.1016/j.molstruc.2025.144281.
[17] Singh M, Takawale S, Patil R, Chaudhari S, Pathan A, Sangshetti J, et al. Development and Characterization of Co-crystals Assisted with In-silico Screening for Solubility and Permeability Enhancement of Curcumin 2023:2023.09.08.556876. https://doi.org/10.1101/2023.09.08.556876.
[18] Guan H, Sun H, Zhao X. Application of Density Functional Theory to Molecular Engineering of Pharmaceutical Formulations. Int J Mol Sci 2025;26:3262. https://doi.org/10.3390/ijms26073262.

[19] Babar V, Sharma S, Shaikh AR, Oliva R, Chawla M, Cavallo L. Sensing Hachimoji DNA Bases with Janus MoSH Monolayer Nanodevice: Insights from Density Functional Theory (DFT) and Non-Equilibrium Green's Function Analysis. ACS Omega 2024;9:48173–84. https://doi.org/10.1021/acsomega.4c05356.
[20] Devi S, Kumar A, Kapoor A, Verma V, Yadav S, Bhatia M. Ketoprofen–FA Co-crystal: In Vitro and In Vivo Investigation for the Solubility Enhancement of Drug by Design of Expert. AAPS PharmSciTech 2022;23:101. https://doi.org/10.1208/s12249-022-02253-5.
[21] Elshahat A, Hasan AA, Elghamry HA, Balata GF. Formulation and optimization of olanzapine-carboxylic acid cocrystals orodispersible tablets: In-vitro/ In-vivo study. J Drug Deliv Sci Technol 2024;100:106093. https://doi.org/10.1016/j.jddst.2024.106093.
[22] Jha R, Patel S, Sekhani A, Parmar HA, Desai N, Shah P. Rational Design of Amiodarone Co-crystals: A Synergistic Strategy Combining Computational Prediction, Precipitation-Inhibiting Polymers, and Formulation Optimisation. AAPS PharmSciTech 2026;27:123. https://doi.org/10.1208/s12249-026-03361-2.
[23] Kara DD, Bangera PD, Keerikkadu M, Rathnanand M. Integrative green synthesis and molecular simulation of ibrutinib cocrystals for enhanced biopharmaceutical performance and in vivo pharmacokinetics. Int J Pharm X 2025;10:100371. https://doi.org/10.1016/j.ijpx.2025.100371.
[24] Dayo Owoyemi BC, Zeller M, Pereira da Silva B, Akinyemi AO, Ando RA, de Araujo GLB, et al. Drug Property Optimization: Design, Synthesis, and Characterization of Novel Pharmaceutical Salts and Cocrystal-Salt of Lumefantrine. Mol Pharm 2025;22:1042–60. https://doi.org/10.1021/acs.molpharmaceut.4c01244.
[25] Wong SN, Weng J, Ip I, Chen R, Lakerveld R, Telford R, et al. Rational Development of a Carrier-Free Dry Powder Inhalation Formulation for Respiratory Viral Infections via Quality by Design: A Drug-Drug Cocrystal of Favipiravir and Theophylline. Pharmaceutics 2022;14:300. https://doi.org/10.3390/pharmaceutics14020300.
[26] Vyas G, Shah J, Jacob S. DoE implementation for Telmisartan and hydrochlorothiazide drug-drug cocrystal synthesis to enhance physicochemical and pharmacokinetic properties. J Appl Pharm Sci 2023;13,:067–76. https://doi.org/10.7324/JAPS.2023.90012.
[27] Marcos Valdez MM, Sperandeo NR, Bueno MS, Garnero C. Pharmaceutical Cocrystals in Drug-Delivery Technologies: Advances from Rational Design to Therapeutic Applications. Pharmaceutics 2026;18:128. https://doi.org/10.3390/pharmaceutics18010128.
[28] Li M, Wang J, Xu X, Ren G, Zhu B, Hong M, et al. Study of Cycloxaprid Co-crystals: Characterization, Theory Calculation, Solubility, and Stability. Cryst Growth Des 2022;22:4437–52. https://doi.org/10.1021/acs.cgd.2c00394.
[29] Yu Y-M, Li X-J, Bu F-Z, Zhao Z-L, Wu Z-Y, Li Y-T. Drug–Drug Cocrystal Alloy and Nanoformulation of Cytarabine: Optimized Biopharmaceutical Property and Synergistic Antitumor Efficacy. Mol Pharm 2024;21:5716–27. https://doi.org/10.1021/acs.molpharmaceut.4c00733.
[30] Dhibar M, Chakraborty S, Basak S, Pattanayak P, Chatterjee T, Ghosh B, et al. Critical Analysis and Optimization of Stoichiometric Ratio of Drug-Coformer on Cocrystal Design: Molecular Docking, In Vitro and In Vivo Assessment. Pharmaceuticals 2023;16:284. https://doi.org/10.3390/ph16020284.
[31] Sukumaran J, Priya M, Venkatesan R, Sathiasivan K, Khan MR, Kim S-C. Green Synthesis of Nickel Oxide Nanoparticles Using Leaf Extract of Aegle marmelos and Their Antibacterial, Anti-Oxidant, and In Vitro Cytotoxicity Activity. Microsc Res Tech 2025;88:2830–42. https://doi.org/10.1002/jemt.70054.

[32] Kumar S, Singh R, Dutta D, Chandel S, Bhattacharya A, Ravichandiran V, et al. In Vitro Anticancer Activity of Methanolic Extract of Justicia adhatoda Leaves with Special Emphasis on Human Breast Cancer Cell Line. Molecules 2022;27:8222. https://doi.org/10.3390/molecules27238222.
[33] Palanisamy S, David R, Madav E, Devi Kannan V, Rajendran V, Sampath S, et al. Green fabrication of silver nanoparticles using leaf extract of tropical vine Momordica charantia: spectral characterization and in vitro cytotoxicity evaluation on human breast cancer cells. Mater Technol 2024;39:2304428. https://doi.org/10.1080/10667857.2024.2304428.
[34] Liang X, Liu S, Li Z, Deng Y, Jiang Y, Yang H. Efficient cocrystal coformer screening based on a Machine learning Strategy: A case study for the preparation of imatinib cocrystal with enhanced physicochemical properties. Eur J Pharm Biopharm 2024;196:114201. https://doi.org/10.1016/j.ejpb.2024.114201.
[35] Shaik A, Bhagwat PU, Palanisamy P, Chhabria D, Dubey P, Kirubakaran S, et al. Novel pharmaceutical co-crystals of gefitinib: synthesis, dissolution, cytotoxicity, and theoretical studies. CrystEngComm 2023;25:2570–81. https://doi.org/10.1039/D3CE00056G.
[36] A Novel Solid Form of Erlotinib: Synthesis by Heterogeneous Complexation and Characterization by NMR Crystallography. Cryst Growth Des 2025.
[37] Reggane M, Wiest J, Saedtler M, Harlacher C, Gutmann M, Zottnick SH, et al. Bioinspired co-crystals of Imatinib providing enhanced kinetic solubility. Eur J Pharm Biopharm 2018;128:290–9. https://doi.org/10.1016/j.ejpb.2018.05.012.
[38] Basavoju S, Boström D, Velaga SP. Indomethacin–Saccharin Cocrystal: Design, Synthesis and Preliminary Pharmaceutical Characterization. Pharm Res 2008;25:530–41. https://doi.org/10.1007/s11095-007-9394-1.
[39] Dhibar M, Chakraborty S, Basak S, Pattanayak P, Chatterjee T, Ghosh B, et al. Critical Analysis and Optimization of Stoichiometric Ratio of Drug-Coformer on Cocrystal Design: Molecular Docking, In Vitro and In Vivo Assessment. Pharmaceuticals 2023;16:284. https://doi.org/10.3390/ph16020284.
[40] Thakuria R, Sarma B. Drug-Drug and Drug-Nutraceutical Cocrystal/Salt as Alternative Medicine for Combination Therapy: A Crystal Engineering Approach. Crystals 2018;8:101. https://doi.org/10.3390/cryst8020101.
[41] Masuda Y, Kato K. Nanocrystal Assembled TiO_2 Particles Prepared from Aqueous Solution. Cryst Growth Des 2008;8:3213–8. https://doi.org/10.1021/cg701103u.
[42] Imanto T, Wikantyasning ER, Nurwaini S, Amalia M, Sambudi NS, Harun NY. PREPARATION AND SOLID-STATE CHARACTERIZATION OF KETOPROFEN-SUCCINIC ACID-SACCHARIN CO-CRYSTAL WITH IMPROVED SOLUBILITY. Int J Appl Pharm 2024:275–9. https://doi.org/10.22159/ijap.2024v16i1.48829.
[43] Babu NJ, Nangia A. Solubility Advantage of Amorphous Drugs and Pharmaceutical Cocrystals. Cryst Growth Des 2011;11:2662–79. https://doi.org/10.1021/cg200492w.
[44] Marcos Valdez MM, Sperandeo NR, Bueno MS, Garnero C. Pharmaceutical Cocrystals in Drug-Delivery Technologies: Advances from Rational Design to Therapeutic Applications. Pharmaceutics 2026;18:128. https://doi.org/10.3390/pharmaceutics18010128.
[45] Su W, Shen S, Peng J, Wu D, Liu X, Deng Y, et al. Study on Novel Solid-State Forms of Sorafenib with Advantages in Terms of Solubility 2023. https://doi.org/10.20944/preprints202311.1082.v1.
[46] Sarabia-Vallejo Á, Caja M del M, Olives AI, Martín MA, Menéndez JC. Cyclodextrin Inclusion Complexes for Improved Drug Bioavailability and Activity: Synthetic and

Analytical Aspects. Pharmaceutics 2023;15:2345. https://doi.org/10.3390/pharmaceutics15092345.
[47] Červinka C, Fulem M. Structure and Glass Transition Temperature of Amorphous Dispersions of Model Pharmaceuticals with Nucleobases from Molecular Dynamics. Pharmaceutics 2021;13:1253. https://doi.org/10.3390/pharmaceutics13081253.

Supplementary Files

This is a list of supplementary files associated with this preprint. Click to download.

- SupplemnetoryData1.docx